

Photometric Observations of Star Formation Activity in Early Type Spirals

Tadashi Usui and Mamoru Saitō

Department of Astronomy, Faculty of Science, Kyoto University

Sakyo-ku, Kyoto 606-8502, Japan

Electronic mail: usui, saitom@kusastro.kyoto-u.ac.jp

Akihiko Tomita

Department of Earth and Astronomical Sciences, Faculty of Education,

Wakayama University, Wakayama 640-8510, Japan

Electronic mail: atomita@center.wakayama-u.ac.jp

Received _____; accepted _____

ABSTRACT

We observationally study the current star formation activities of early type spiral galaxies. We construct a complete sample of 15 early type spirals having far-infrared (FIR) to optical B band luminosity ratios, $\log(L_{\text{FIR}}/L_B)$, larger than the average of the type, and make their CCD imaging of the R and $\text{H}\alpha$ bands. The equivalent widths of $\text{H}\alpha$ emission increase with increasing L_{FIR}/L_B , indicating that $\log(L_{\text{FIR}}/L_B)$ can be an indicator of star formation for such early type spirals with star formation activities higher than the average. For all of the observed early type spirals, the extended H II regions exist at the central regions with some asymmetric features. $\text{H}\alpha$ emission is more concentrated to the galactic center than the R band light, and the degree of the concentration increases with the star formation activity. We also analyze the relation between the star formation activities and the existence of companion galaxies in the sample galaxies and other bright early type spirals. No correlation is found and this suggests that the interaction is not responsible for all of the star formation activities of early type spirals.

Subject headings: galaxies: spiral — galaxies: photometry — galaxies: starburst — galaxies: interactions

1. Introduction

Kennicutt *et al.* (1994) extended the study of star formation activities of spiral galaxies by Kennicutt (1983), and showed that the ratio of the current star formation rate (SFR) to the average past SFR increases as the morphological type becomes later, from 0.01 in Sa to 1 in Sc. They used the integrated $H\alpha$ equivalent width (EW) as an indicator of star formation activity. Their samples were about 200 galaxies, in which galaxies having active galactic nuclei (AGNs) or interacting companions were not included.

On the other hand, far-infrared (FIR) luminosity of spiral galaxies is considered to be another indicator of the current SFR. A luminosity function of $60\ \mu\text{m}$ emission obtained by the *IRAS* is similar for galaxies from Sa to Scd (Devereux & Young 1991). FIR to optical B band luminosity ratio, $\log(L_{\text{FIR}}/L_B)$, has been used as an indicator of the present star formation activity of spiral galaxies by many researchers (e.g., de Jong *et al.* 1984, Bothun *et al.* 1989, Tomita *et al.* 1996, Devereux & Hameed 1997). Tomita *et al.* (1996) constructed a histogram of $\log(L_{\text{FIR}}/L_B)$ for each morphological type, and showed that the distribution is rather flat from -1.5 to 0.5 in early type spirals (Sa-Sab), while it is much concentrated within 1 dex around -0.5 in late type spirals (Sc). These suggest that there are many early type spirals with high star formation activities, in contrast with the result of Kennicutt *et al.* (1994).

There is, however, a controversy over the origin of FIR emission of spiral galaxies. FIR emission generally consists of at least two components: a warm component from dust in star forming region and a cool component from diffuse interstellar dust, heated by the general interstellar radiation field (e.g., Helou 1986). Devereux & Young (1990) investigated the relation between FIR and $H\alpha$ luminosity and showed that high-mass stars are responsible for the both luminosities. The morphological dependence of the ratio of FIR to $H\alpha$ luminosity was investigated by Sauvage & Thuan (1992). Their ratios systematically decrease from early to late type spirals, and they interpreted this trend as the decreasing contribution of cirrus component, from about 86% for Sa galaxies to about 3% for Sdm galaxies. Xu (1990) analyzed intensities of UV (at $2000\ \text{\AA}$) and FIR emission for about 40 spirals, most of which are late type, and concluded

that the cool component is dominantly due to the non-ionizing UV radiation from intermediate massive stars ($\sim 5 M_{\odot}$) with lifetimes of the order of 10^8 yr (see also Walterbos & Greenawalt 1996). Moreover, there is a tight and universal correlation between the integrated FIR and radio continuum emission, most of which is non-thermal, for various types of galaxies from Sa to Sm (Wunderlich *et al.* 1987). The radio continuum is generated by the synchrotron radiation of cosmic ray electron, and cosmic rays are accelerated by supernova explosions, whose progenitor is also responsible for FIR emission (Lisenfeld *et al.* 1996). This correlation further supports the notion that FIR emission is a star formation indicator as well as $H\alpha$ emission.

The sample of early type spirals of Kennicutt (1983) and Kennicutt (1992), on which Sauvage & Thuan (1992) and Kennicutt *et al.* (1994) were based, is small in number and may be biased to the galaxies with low values of $\log(L_{\text{FIR}}/L_B)$. Caldwell *et al.* (1991) studied star formation activities of Sa galaxies, selected from the Revised Shapley-Ames Catalog (Sandage & Tammann 1987). But most of their galaxies are weak in FIR emission, i.e., $\log(L_{\text{FIR}}/L_B) < -1.0$, and half of their sample are classified as earlier than Sa in the Third Reference Catalog of Bright Galaxies (RC3; de Vaucouleurs *et al.* 1991). Recently Young *et al.* (1996) presented the $H\alpha$ emission line flux of spiral galaxies extensively, but the sample is still small in number for early type spirals with high values of $\log(L_{\text{FIR}}/L_B)$.

In this study we make CCD imaging of the R and $H\alpha$ bands for 15 early type spirals with $\log(L_{\text{FIR}}/L_B) \geq -0.5$ and investigate the properties of FIR emission as an indicator of star formation activity by comparing with $H\alpha$ emission. $H\alpha$ emission originates exclusively from newly born massive stars, aside from AGN, and connects directly with the present star formation activities, though the effect of the extinction remains uncertain. Moreover the $H\alpha$ images provide some insights about the distribution of star forming regions. We describe the sample selection, observations and data reduction in § 2. In § 3, after comments on individual galaxies, we show that $\log(L_{\text{FIR}}/L_B)$ can be a star formation indicator comparable to $H\alpha$ luminosity for early type spirals with higher star formation activities. We also show the trend of the central concentration of the star forming regions in the observed galaxies. In § 4 we discuss the difference of star

formation indicators between FIR and H α emission, and estimate a general distribution of H α EW of early type spirals. We also analyze the effect of galaxy-galaxy interactions on the star formation activities in early type spirals. A summary is given in § 5.

2. Data

2.1. Galaxy Sample

In this paper we refer early type spirals as galaxies with morphological types Sa and Sab, or $0.5 \leq T < 2.5$ for the index of the Hubble sequence given in RC3.

We select early type spirals having B_T^0 and $(B - V)_T^0$ in RC3 and $\log(L_{\text{FIR}}/L_B) \geq -0.5$. The range of $\log(L_{\text{FIR}}/L_B)$ adopted here represents that the selected galaxies have $\log(L_{\text{FIR}}/L_B)$ higher than the average of early type spirals. The values of $\log(L_{\text{FIR}}/L_B)$ are computed using B_T^0 in RC3 and 60 μm and 100 μm flux densities of *IRAS* data in the same manner as that of Tomita *et al.* (1996). The FIR luminosity, L_{FIR} , in solar units is given by Lonsdale *et al.* (1985) as

$$\log L_{\text{FIR}} = \log(2.58f_{60} + f_{100}) + 2\log D + 5.595, \quad (1)$$

where D is the distance in Mpc, assuming $H_0 = 75 \text{ km s}^{-1} \text{ Mpc}^{-1}$, f_{60} and f_{100} are the flux densities at 60 μm and 100 μm in Jy. Following Soifer *et al.* (1987), the B band luminosity, L_B , in solar units is given as

$$\log L_B = -0.4B_T^0 + 2\log D + 11.968. \quad (2)$$

The additional criteria of our sample are as follows: they are (1) nearby galaxies with recession velocities $1000 \text{ km s}^{-1} \leq cz \leq 2600 \text{ km s}^{-1}$, (2) at the declination range $-15^\circ \leq \delta \leq 70^\circ$, (3) with optical diameters $\leq 4.0'$ to secure sufficient sky area in each CCD image, (4) rather face-on with inclination $\leq 60^\circ$, which suffers less extinction in H α luminosity (Young *et al.* 1996), and (5) without Seyfert activity. The sample selection is not related to the presense of a bar nor a sign of interaction, because our main purpose is to obtain the relation between H α and FIR emission of early type spirals as a whole.

The complete sample consists of 15 galaxies, which are given in Table 1 along with the properties. B_T^0 of the sample galaxies ranges from 11.5 to 13.6. The range of optical diameters is from 10 kpc to 20 kpc, except for two small galaxies and one large galaxy. Seven sample galaxies were previously identified as Markarian or Kiso Ultraviolet Excess Galaxies (KUGs), as shown in the 15th column of Table 1. They are UV-bright and suggest higher star formation activities. Nuclear spectra have been known to be the H II region type for 8 of our sample galaxies in the literature (column 13 of Table 1).

We also observed other 6 spiral galaxies regardless of morphological type for a comparison, H α EWs of which had been measured by other researchers. These galaxies are listed in Table 2 with the properties. NGC 681 is one of our sample galaxies, and the H α EW of the galaxy was measured by Kennicutt (1983). So we use this galaxy as a comparison galaxy.

2.2. Observations and Data Reduction

The observations were made using a CCD camera (Thomson 7882, 576×384 pixels) attached to the Cassegrain focus of the 0.6 m reflector (focal length = 4.8 m) at the Ouda Observatory, Kyoto University (Ohtani *et al.* 1992) between 1996 December and 1998 March. The scale was $1.''0$ per pixel and the field of view was $10' \times 6'$. Seeing during the run was around $5''$. To measure H α + [N II] emission line intensities, we observed each galaxy using two filters, i.e., a narrow band filter ($\lambda_c = 6610 \text{ \AA}$, $\Delta\lambda = 80 \text{ \AA}$), which covers H α + [N II] emission for galaxies with recession velocities between 1000 km s^{-1} and 3500 km s^{-1} , and a broad R band filter with a band width of $\sim 1000 \text{ \AA}$, which gives the continuum intensity around the emission lines. The integration time for each frame was 2 to 4 min, and the total integration time of each object was 1 to 2 h in the narrow band and 10 to 20 min in the R band.

Standard CCD reductions were performed using IRAF¹. The images were bias-subtracted

¹IRAF is the software developed in National Optical Astronomy Observatories.

and flat-fielded using a frame of twilight sky. Then the images were sky-subtracted, aligned and scaled using foreground stars, and median-combined to make the final image of each galaxy in the both narrow and R band. To determine the continuum level, the R band image was scaled by the ratio of the count of the foreground stars of the R band image to that of the narrow band image. The scaled R band image was subtracted from the narrow band image, and the pure $\text{H}\alpha + [\text{N II}]$ emission line image was yielded. We determined the continuum level with an error of around 5%. The uncertainty depended on mainly the number of foreground stars in each image.

We obtained the EW of $\text{H}\alpha + [\text{N II}]$ emission lines as the ratio of the $\text{H}\alpha + [\text{N II}]$ emission line flux to the continuum flux in the aperture which was taken from D_{25} in RC3. $[\text{N II}]/\text{H}\alpha$ ratio in the integrated light of each galaxy is considered to be similar from galaxy to galaxy (Kennicutt & Kent 1983). So we did not correct for the $[\text{N II}]$ emission, and hereafter we refer the EW of $\text{H}\alpha + [\text{N II}]$ emission lines as $\text{H}\alpha$ EW or $\text{EW}(\text{H}\alpha)$. The second column of Table 3 shows the $\text{H}\alpha$ EWs with the uncertainties for the sample galaxies as well as the comparison galaxies. The uncertainties were derived in two ways; one is from the statistics of the sky level and the scaling factor to determine the continuum level, and another is from the internal disagreement of different nights' observations of the galaxy. In most cases the two uncertainties were comparable; if they were significantly different, the larger value is listed in Table 3.

We estimated $\text{H}\alpha + [\text{N II}]$ emission line flux, which hereafter we refer as $f_{\text{H}\alpha}$, in the following manner. The R magnitude has not given for most of the sample galaxies, but all of the observed galaxies have B_T and V_T . First, we constructed the $(B - V)_T - (V - R)_T$ diagram by combining the data of $(B - V)_T$ in RC3 and $(V - R)_T$ in Buta & Williams (1995) for mostly normal galaxies. Then we estimated the R magnitude from B_T and V_T , using the equation: $R_T = V_T - (V - R)_T = V_T - 0.37(B - V)_T - 0.23 \pm 0.05$. We converted the R magnitude to the flux density, and assumed it to be the continuum flux density around the $\text{H}\alpha$ line. $f_{\text{H}\alpha}$ was computed from $\text{H}\alpha$ EW and the flux density. $\text{H}\alpha + [\text{N II}]$ luminosity in solar units, which hereafter we refer as $L_{\text{H}\alpha}$, was also estimated after the correction for the Galactic extinction. The Galactic extinction in B band, A_g , in RC3 was converted to the extinction at $\text{H}\alpha$ line, assuming $A(\text{H}\alpha)/A_g = 0.61$.

We did not correct for the internal extinction nor [N II] emission. The estimated $f_{\text{H}\alpha}$ and $L_{\text{H}\alpha}$ are given in the third and fourth columns of Table 3, respectively. $L_{\text{H}\alpha}$ of the sample galaxies are of the order of $10^7 L_{\odot}$. The data of Ho *et al.* (1997) showed that $L_{\text{H}\alpha}$ of LINERs are less than $2 \times 10^6 L_{\odot}$ for all of the observed 28, except one, early type spirals. So in our sample galaxies the contribution of LINERs, if any, is probably negligible in the $L_{\text{H}\alpha}$.

We also measured half-light radii of the R band continuum and $\text{H}\alpha$ emission, $r_{e,R}$ and $r_{e,\text{H}\alpha}$, respectively, to gauge the distribution of light within a galaxy. The half-light radii were defined such the radius that the circular aperture of $r_{e,R}$ ($r_{e,\text{H}\alpha}$) encompasses a half of the total flux of R ($\text{H}\alpha$) band light of the galaxy. The measurements on the different nights’ imagings of each galaxy agree quite well. We calculated the ratio of $r_{e,\text{H}\alpha}$ to r_{25} and the ratio of $r_{e,\text{H}\alpha}$ to $r_{e,R}$, where r_{25} is the optical radius of the galaxy and equal to a half of D_{25} . $r_{e,\text{H}\alpha}/r_{25}$ indicates the degree of the concentration of $\text{H}\alpha$ emission relative to the optical size of the galaxy, and $r_{e,\text{H}\alpha}/r_{e,R}$ indicates the degree of the concentration of $\text{H}\alpha$ emission relative to the continuum light. We tabulate $r_{e,\text{H}\alpha}$ in kpc, $r_{e,\text{H}\alpha}/r_{25}$, and $r_{e,\text{H}\alpha}/r_{e,R}$ in the last three columns of Table 3.

3. Results

3.1. Comparison with Previous Studies

We observed 7 galaxies listed in Table 2 with known $\text{H}\alpha$ EWs. Figure 1 shows a comparison of $\text{H}\alpha$ EWs measured by us with those measured by Kennicutt (1983) and Romanishin (1990). Their measurements were made by using large aperture ($1'$ to $7'$) photometry. The $\text{H}\alpha$ EWs of Kennicutt (1983) were corrected by a factor 1.16 following by Kennicutt *et al.* (1994). The mean error is :

$$\Delta[\text{EW}(\text{H}\alpha) \text{ (this study)} - \text{EW}(\text{H}\alpha) \text{ (other studies)}] = 2.6 \pm 6.7 \text{ \AA}. \quad (3)$$

Our values of $\text{H}\alpha$ EWs thus agree with the values obtained by others for $\text{EW}(\text{H}\alpha) > 20 \text{ \AA}$; most of the sample galaxies have $\text{H}\alpha$ EWs in this range, as shown in Table 3. NGC 681 has relatively weak $\text{H}\alpha$ EWs and the difference between Kennicutt’s (1983) and ours is the largest. This galaxy is one

of our sample, and the physical values derived from the two H α EWs shall be shown hereafter.

We also compared our estimated $f_{\text{H}\alpha}$ with the values of Kennicutt (1983) and Romanishin (1990), and the ratio is :

$$\log \left[\frac{f_{\text{H}\alpha} \text{ (this study)}}{f_{\text{H}\alpha} \text{ (other studies)}} \right] = -0.03 \pm 0.09. \quad (4)$$

These errors are small enough for the following discussion.

3.2. Description of Individual Galaxies

The images of 15 sample galaxies observed by us are shown in Figure 2. For each galaxy, the R band image is left and the H α image is right. North is at the top and east is at the left. The intensity is scaled logarithmically. Though the resolution of our images is around $5''$, it is apparent that there are much variety in H α properties. We describe the images of individual galaxies briefly.

NGC 681. The inclination of NGC 681 estimated is small and close to the critical value of our sampling. The H α emission is strong in the central region and extended along the disk. A dust lane is seen on the north of the center. The bright object at the north-western edge of this galaxy is a foreground star.

NGC 1022. In the Carnegie Atlas of Galaxies (Sandage & Bedke 1994, the Carnegie Atlas), thin dust filaments are seen within the ring, but they cannot be seen in our R band image because of the poor resolution. The H α emission is concentrated to the central region.

NGC 2782. This galaxy is sometimes classified as a Seyfert galaxy, but Boer *et al.* (1992) showed that the nuclear spectrum is typical of nuclear starbursts and the high excitation gas due to shocks is on the $4''$ to $8''$ south of the center. In the Carnegie Atlas, low surface brightness components extend far beyond D_{25} , and fragments of dust lanes in spiral arms exist through the central bulge. Smith (1994) considered this galaxy is merging with a dwarf galaxy. H α emission is strong in the central region and also seen on the north-western arc. The southern component which corresponds to the high excitation gas is weak in H α emission compared with the center.

NGC 2993. This galaxy is strongly interacting with NGC 2992, which is at the $3'$ north-west of the galaxy. Tidal tails are seen in our original image and the Carnegie Atlas. Star formation occurs in the central region, and diffuse $H\alpha$ emission surrounds it.

NGC 3442. This galaxy is small and less luminous. No feature is seen in the R band image. In the $H\alpha$ image two discrete H II regions are seen across the nucleus.

NGC 3504. The $H\alpha$ emission is strong in the galactic center and also on the inner ring. The brightest part on the ring coincides with the southern end of the bar. There is a companion galaxy, NGC 3512, at $12'$ east of this galaxy. This galaxy is extensively studied by Kenney *et al.* (1993).

NGC 3611. This galaxy has a companion galaxy UGC 6306 at the south with a separation of $3'$. The $H\alpha$ emission is concentrated to the central region, and the emission region extends toward south.

NGC 3729. Both the R and $H\alpha$ images of this galaxy resemble NGC 3504, though the star formation activity is weaker than that galaxy. The bright object at the southern edge of this galaxy is a foreground star.

NGC 4045. In the R band image the outer envelope is rather oval, but the inner ring is almost circular. The inner ring is also traceable in $H\alpha$ emission. The brightest H II region is at the galactic center. NGC 4045A ($cz = 5329 \text{ km s}^{-1}$), which appears on the southern edge of this image, does not have a physical relation with the galaxy.

NGC 4369. The R band image is featureless. Discrete two H II regions are resolved around the galactic center, but the galactic center itself is faint in $H\alpha$ emission.

NGC 4384. Two major H II regions are seen symmetrically with respect to the galactic center, and diffuse $H\alpha$ emission surrounds them. In the *HST* image, spiral structure reaches down to the center, and several bright sources, likely H II regions, can be seen (Carollo *et al.* 1997).

NGC 5534. This galaxy may be in the process of merger (see the Carnegie Atlas). The strong $H\alpha$ emission is in the central region, and there are emission regions at the western side of the

galaxy. The companion galaxy is located at the eastern side and also shows $H\alpha$ emission.

NGC 5691. In the R band image, there is a dust lane at the north-west of the galactic center. The H II regions are seen at the central region.

NGC 5915. This galaxy is interacting with NGC 5916 and NGC 5916A, which are located at $5'$ south and $5'$ west of the galaxy, respectively. The $H\alpha$ emission is seen on the entire galaxy and the brightest H II region is on the southern arm, which is on the side of NGC 5916.

NGC 7625. This galaxy has a tube-like dust lane in the Carnegie Atlas, which cannot be seen in our R band image. Patchy H II regions and more diffuse emission are seen in the $H\alpha$ image. This Arp galaxy occurs intense star formation, but does not have any companion galaxy. Li *et al.* (1993) observed and studied this galaxy extensively.

The early type spirals observed in the present study have the extended H II regions at the central regions with some asymmetric features. The intensities at faint extended $H\alpha$ emission are well above the errors estimated from the uncertainties of continuum subtraction and scaling factor between $H\alpha$ and R band image, and these features are real. For some of barred or ringed galaxies, e.g., NGC 3504, NGC 4045, the star formation also takes place on the ends of a bar or a ring. Nevertheless it is at the central region that the star formation takes place most intensely. The degree of the concentration of the H II regions to the galactic center is discussed quantitatively in § 3.4.

3.3. Correlation between $EW(H\alpha)$ with L_{FIR}/L_B

In Figure 3 we plot the $\log[EW(H\alpha)]$ versus $\log(L_{FIR}/L_B)$ relation for 15 sample early type spirals by filled circles as well as 16 early type spirals of Kennicutt (1983, 1992) by open circles. For their galaxies having two data, we adopted the mean $H\alpha$ EW. We show two $H\alpha$ EWs of NGC 681 obtained by us and Kennicutt (1983), and connected each data point by a vertical line. The mean of the two values is also shown by a cross. In Figure 3 there is a trend that $\log[EW(H\alpha)]$

increases with increasing $\log(L_{\text{FIR}}/L_B)$. A least-squares fit yields

$$\log[\text{EW}(\text{H}\alpha)] = 0.82\log(L_{\text{FIR}}/L_B) + 1.48, \quad (5)$$

and the correlation coefficient is 0.79, provided that we excluded galaxies with $\text{EW}(\text{H}\alpha) \leq 3 \text{ \AA}$ from the fit because of the large errors of $\text{H}\alpha$ EW in logarithmic scale. Thus $\log(L_{\text{FIR}}/L_B)$ can be a star formation indicator for early type spirals with higher star formation activities. We do not extrapolate the correlation to less active galaxies because of the presence of two sources of the FIR emission, i.e., cirrus and weak H II regions, and difficulty in measurements of weak $\text{H}\alpha$ EW. It can only be said that galaxies with $\log(L_{\text{FIR}}/L_B) < -0.5$ have $\text{H}\alpha$ EWs less than 10 \AA . In § 4.1 we shall interpret the non-linearity and relatively large scatter of the correlation between $\text{H}\alpha$ EW and L_{FIR}/L_B .

3.4. Star Forming Region

We regard $r_{e,\text{H}\alpha}$ listed in Table 3 as a typical radius of star forming region of each galaxy. For the sample galaxies the mean of $r_{e,\text{H}\alpha}/r_{25}$ is 0.15, and $r_{e,\text{H}\alpha}/r_{e,R}$ is less than unity for most of galaxies. The former means that a half of star formation occurs within the inner 15% of the optical radius. The latter means that $\text{H}\alpha$ emission is more concentrated to the central region than the R band light. Ryder & Dopita (1994) observed 34 spiral galaxies, most of which are late type, and showed that the scale length of $\text{H}\alpha$ emission is much longer than the V and I scale length in the outer disk, indicating that $\text{H}\alpha$ emission is *less* concentrated to the galactic center than the broad band light in late type spirals.

In Figure 4 we plot $r_{e,\text{H}\alpha}/r_{e,R}$ as a function of $\log(L_{\text{FIR}}/L_B)$ for our sample galaxies (filled circles). One comparison galaxy, NGC 7217, is classified as an early type spiral but we did not include this galaxy in our sample because of the low value of $\log(L_{\text{FIR}}/L_B)$. We plot the data of NGC 7217 by an open circle for a comparison. In the diagram the galaxies with vertical bar are barred galaxies (SB), and ones with horizontal bar are galaxies with companions. There is a trend that the degree of the concentration increases as the star formation activity is higher. The trend

seems to be not related to the presence of companion nor bar structure. Lehnert & Heckman (1996) reported that $r_{e,H\alpha}/r_{e,R}$ is weakly correlated with the FIR color but not correlated with the ratio of IR-to- B band luminosity for more actively star forming galaxies than ours. But the high extinction and the edge-on nature of their sample may blur the correlation if it exists.

4. Discussion

4.1. Difference of the Star Formation Indicators in $H\alpha$ and FIR

Though L_{FIR}/L_B correlates with $H\alpha$ EW (see Figure 3), there are some differences between $H\alpha$ and FIR emission as the star formation indicators. Figure 5 shows $\log(L_{\text{FIR}}/L_{H\alpha})$ as a function of $\log(L_{\text{FIR}}/L_B)$ for early type spirals with $\log(L_{\text{FIR}}/L_B) \geq -0.5$ of our sample (filled circles) and the sample of Kennicutt (1983, 1992) (open circles), which have $\text{EW}(H\alpha) \geq 10 \text{ \AA}$, except for two Kennicutt’s objects including NGC 681 (see Figure 3). For the objects of Kennicutt (1992), we estimated $f_{H\alpha}$ from $H\alpha$ EW by the same manner as described in § 2.2. NGC 4750 has no $(B-V)_T$ data in RC3, and we omitted the galaxy from their sample. $L_{H\alpha}$ was corrected for the Galactic extinction and not corrected for the internal extinction nor $[\text{N II}]$ emission. For the plotted galaxies, there is a trend that $\log(L_{\text{FIR}}/L_{H\alpha})$ increases with $\log(L_{\text{FIR}}/L_B)$ with a correlation coefficient of 0.60; as the star formation activity is higher, $H\alpha$ emission tends to become weaker compared with FIR emission. This trend corresponds to the fact that the slope of Figure 3 is less than unity, as shown in equation (5). The feature originates due to the heavier obscuration for younger stellar objects. Wood & Churchwell (1989) found that in the Galaxy O stars are obscured in the parent molecular clouds during a time of 10% to 20% of the life; in the process of star formation L_{FIR} grows faster than $L_{H\alpha}$. Parent interstellar matter removes from young massive stars with time, the intensities of FIR emission reduce, and the H II regions become apparent. So $L_{H\alpha}$ begins to grow later than L_{FIR} and is increasing even at the phase that $\log(L_{\text{FIR}}/L_B)$ is decreasing.

On the other hand, Figure 4 suggests that in our sample galaxies the more active star

formation occurs in the more concentrated region. This concentration may also affect the value of $\log(L_{\text{FIR}}/L_{\text{H}\alpha})$. In Figure 6 we plot $\log(L_{\text{FIR}}/L_{\text{H}\alpha})$ and $r_{e,\text{H}\alpha}/r_{e,R}$ for our sample early type spirals (filled circles) and a comparison early type spiral (open circle). Although the correlation between the two parameters is marginal, there is a weak trend that the higher central concentration (i.e., lower $r_{e,\text{H}\alpha}/r_{e,R}$) leads to the higher $\log(L_{\text{FIR}}/L_{\text{H}\alpha})$. The extinction for H α emission possibly becomes higher towards the galactic centers.

The value of $\log(L_{\text{FIR}}/L_{\text{H}\alpha})$ thus depends on both the phase of the star formation and the extinction for early type spirals with higher star formation activities, and the both effects yield the non-linearity and the relatively large scatter of the correlation between L_{FIR}/L_B and H α EW in Figure 3.

4.2. Distribution of H α EW of Early Type Spirals

Tomita *et al.* (1996) made a universal histogram of $\log(L_{\text{FIR}}/L_B)$ for each morphological type. We divide H α EW into three ranges: 0 - 10 Å, 10 - 20 Å, and over 20 Å. For early type spirals the range of $\text{EW}(\text{H}\alpha) = 10 - 20$ Å corresponds to $\log(L_{\text{FIR}}/L_B) \simeq -0.47$ to 0, and the range of $\text{EW}(\text{H}\alpha) > 20$ Å corresponds to $\log(L_{\text{FIR}}/L_B) > 0$, from equation (5). The universal histogram of $\log(L_{\text{FIR}}/L_B)$ by Tomita *et al.* (1996) indicates that the relative frequency of the two ranges of H α EW are, respectively, 17% and 29% for early type spirals. Because of the scatter of the relation between H α EW and L_{FIR}/L_B , the conversion of H α EW to $\log(L_{\text{FIR}}/L_B)$ may not be so straightforward, and this estimation is rather crude. These values suggest, however, that the star formation activity of early type spirals is low [$\text{EW}(\text{H}\alpha) \leq 10$ Å] for half or somewhat more galaxies, and the star formation activity is modest or strong [$\text{EW}(\text{H}\alpha) \geq 20$ Å] for about 30% of early type spirals. The star formation activity of early type spirals as a whole is lower than that of late type spirals, H α EWs of which are around 30 Å (Kennicutt 1983), but the difference is not so large as Kennicutt *et al.* (1994) showed. The sample which they used is biased to the galaxies with $\log(L_{\text{FIR}}/L_B) \leq -0.5$ (see Figure 3), while the average of $\log(L_{\text{FIR}}/L_B)$ is -0.5 for early type spirals.

4.3. Relation between the Star Formation Activities and Galaxy Interactions

Galaxy-galaxy interactions are considered to be an important triggering mechanism for starburst galaxies (see a review by Barnes & Hernquist 1992). Both the integrated H α emission and the FIR emission are systematically enhanced in the strongly interacting systems like galaxies in the Atlas of Peculiar Galaxies (Arp 1966), but enhancements are subtle for nearby pair galaxies (Kennicutt *et al.*, 1987). We examine the relation between interactions and star formation activities in nearby early type spirals by the same method as that of Dahari (1985). We assume that the tidal force is proportional to $M_C M_P^{-1} r^{-3}$, where M_P and M_C are the masses of the parent galaxy and its companion, respectively, and r is the spatial separation between the galaxies. We use the B band luminosity instead of the mass of the galaxy. We also assume that the amount of energy exchanged in the encounter is proportional to $|\Delta V|^{-2}$, where ΔV is the relative velocity between the pair members. We can practically know only the projected spatial distance, S , and the velocity difference along the line of sight, $|c\Delta z|$. So we define the interaction parameter (IP) by

$$\text{IP} = \log L_C - \log L_P - 3\log(Sz) - 2\log|c\Delta z|. \quad (6)$$

Here L_C and L_P are the B band luminosity of the companion and the parent galaxy, respectively. If L_C is unknown, we assumed the mass is proportional to $D_{25}^{1.6}$, where D_{25} is the optical diameter in RC3. In this case IP is defined by

$$\text{IP} = 1.6\log D_C - 1.6\log D_P - 3\log(Sz) - 2\log|c\Delta z|, \quad (7)$$

where D_C and D_P are D_{25} given in RC3 of the companion and the parent galaxy, respectively. In this case, IP is identical to Q' in Dahari (1985). IPs derived by above equations are the upper limits in the sense that we adopt the minimum values of ΔV and r .

We searched for companion galaxies within the radius of $10D_P$ and redshift difference less than 1000 km s^{-1} in RC3, and calculated IP for each companion galaxy. If there were two or more companion galaxies in the searched space, we adopted the largest value of IP among IPs calculated for each host-companion galaxy pair. IPs were derived for 87 early type spirals with $B_T^0 \leq 12 \text{ mag}$

in RC3 and for our sample galaxies. The distributions are shown as a function of $\log(L_{\text{FIR}}/L_B)$ in Figure 7(a) and 7(b), respectively. In these diagrams we adopted $\text{IP} = -5$ for galaxies without any companion galaxy. The galaxies with cross in both diagrams of Figure 7 are classified as peculiar in RC3. The peculiar galaxies are considered to have high IP and high $\log(L_{\text{FIR}}/L_B)$; a peculiarity connects with both the presense of companion galaxies and enhanced star formation. In Figure 7, however, the relation between IP and $\log(L_{\text{FIR}}/L_B)$ is random on the whole, and there are star forming early type spirals with neither companion nor peculiarity. There is no companion galaxy for more than half of our sample galaxies as shown in Figure 7(b). We conclude that interactions are not responsible for all of the star formation activities of early type spirals.

On the other hand, bar structures may enhance star formation activities in early type spirals to some extent. Huang *et al.* (1996) showed that $\log(L_{\text{FIR}}/L_B)$ of barred galaxies (SB) is systematically higher than that of un- and weakly-barred galaxies (SA and SAB) only for early type spirals (S0/a - Sbc). But the relation between $r_{e,\text{H}\alpha}/r_{e,R}$ and $\log(L_{\text{FIR}}/L_B)$ is similar regardless of the presence of bars or companion galaxies (see Figure 4). Further observations are needed to fully understand the star formation mechanism(s) of early type spirals.

5. Summary

Kennicutt *et al.* (1994) used $\text{H}\alpha$ EW as an indicator of the present star formation activities and showed that star formation activities of early type spirals are lower than those of late type spirals by a factor of 100. On the other hand, Tomita *et al.* (1996) used $\log(L_{\text{FIR}}/L_B)$ as an indicator of star formation activities, constructed the histogram of $\log(L_{\text{FIR}}/L_B)$ of each morphological type, and suggested that there are many early type spirals with high star formation activities. In order to solve the inconsistency, we made $\text{H}\alpha$ imaging observation of the complete sample of 15 early type spirals with higher $\log(L_{\text{FIR}}/L_B)$ than the average of the type, and have obtained the following conclusions.

1. We have compared $\log(L_{\text{FIR}}/L_B)$ and $\log[\text{EW}(\text{H}\alpha)]$ of early type spirals for 30 early type

spirals consisting of our sample and Kennicutt’s (1983, 1992) sample, and obtained the correlation that L_{FIR}/L_B increases with increasing $\text{H}\alpha$ EW. $\log(L_{\text{FIR}}/L_B)$ can be a star formation indicator for early type spirals with star formation activities higher than the average.

2. For the early type spirals observed by us, the extended H II regions exist at the central regions with some asymmetric features. Additional $\text{H}\alpha$ emission is seen on the ends of a bar or a ring for some barred or ringed galaxies. Even in such cases, it is at the central region that the star formation takes place most intensely. $\text{H}\alpha$ emission is more concentrated to the galactic center than the R band light, and the degree of the concentration increases as the star formation activity is higher.

3. We have found that $\log(L_{\text{FIR}}/L_{\text{H}\alpha})$ tends to increase with increasing of both the activity and the central concentration of the star formation for galaxies with $\log(L_{\text{FIR}}/L_B) > -0.5$. These features are interpreted as the composite effects of the extinction and the phase of the star formation. These effects yield the non-linearity and scatter in the correlation between L_{FIR}/L_B and $\text{H}\alpha$ EW.

4. Our results suggest that star formation activity is modest or strong [$\text{EW}(\text{H}\alpha) \geq 20 \text{ \AA}$] for about 30% of nearby early type spirals as a whole.

5. Only about half of our sample galaxies have companion galaxies. There is no correlation between star formation activities and the degree of the interaction for early type spirals brighter than 12 mag as well as our sample galaxies. This implies that the galaxy interaction is not responsible for all of the star formation activities of early type spirals.

We would like to thank Yuuji Yamamoto, Yoshio Tomita, Taichi Kato and Tsuyoshi Ishigaki for their help with the observations. This research has made use of the NASA/IPAC Extragalactic Database (NED), which is operated by the Jet Propulsion Laboratory, Caltech, under contract with the National Aeronautics and Space Administration.

REFERENCES

- Arp, H. 1966, *Atlas of Peculiar Galaxies* (California Institute of Technology, Pasadena)
- Barnes, J.E., & Hernquist, L. 1992, ARA&A, 30, 705
- Boer, B., Schulz, H., & Keel, W.C. 1992, A&A, 260, 67
- Bothun, G.D., Lonsdale, C.J., & Rice, W. 1989, ApJ, 341, 129
- Buta, R., & Williams, K.L. 1995, AJ, 109, 543
- Caldwell, N., Kennicutt, R., Phillips, A.C., & Schommer, R.A. 1991, ApJ, 370, 526
- Carollo, C.M., Stiavelli, M., de Zeeuw, P.T., & Mack, J. 1997, AJ, 114, 2366
- Contini, T., Considère, S., & Davoust, E. 1998, A&AS, 130, 285
- Dahari, O. 1985, AJ, 90, 1772
- de Jong, T., Clegg, P.E., Soifer, B.T., Rowan-Robinson, M., Habing, H.J., Houck, J.R., Aumann, H.H., & Raimond, E. 1984, ApJ, 278, L67
- de Vaucouleurs, G., de Vaucouleurs, A., Corwin, H.G., Buta, R.J., Patural, G., & Fouqué, P. 1991, Third Reference Catalogue of Bright Galaxies (Springer-Verlag, New York)(RC3)
- Devereux, N.A., & Hameed, S. 1997, AJ, 113, 599
- Devereux, N.A., & Young, J.S. 1990, ApJ, 350, L25
- Devereux, N.A., & Young, J.S. 1991, ApJ, 371, 515
- Durret, F., & Bergeron, J. 1988, A&AS, 75, 273
- Helou, G. 1986, ApJ, 311, L33
- Ho, L.C., Filippenko, A.V., & Sargent, W.L.W. 1997, ApJS, 112, 315

- Huang, J.H., Gu, Q.S., Su, H.J., Hawarden, T.G., Liao, X.H., & Wu, G.X. 1996, *A&A*, 313, 13
- Kenney, J.D.P., Carlstrom, J.E., & Young, J.S. 1993, *ApJ*, 418, 687
- Kennicutt, R.C. 1983, *ApJ*, 272, 54
- Kennicutt, R.C. 1992, *ApJ*, 388, 310
- Kennicutt, R.C., Keel, W.C., van der Hulst, J.M., Hummel, E., & Roettiger, K.A. 1987, *AJ*, 93, 1011
- Kennicutt, R.C., & Kent, S.M. 1983, *AJ*, 88, 1094
- Kennicutt, R.C., Tamblyn, P., & Congdon, C.W. 1994, *ApJ*, 435, 22
- Lehnert, M.D., & Heckman, T.M. 1996, *ApJ*, 472, 546
- Li, J.G., Seaquist, E.R., Wrobel, J.M., Wang, A., & Sage, L.J. 1993, *ApJ*, 413, 150
- Lisenfeld, U., Völk, H.J., & Xu, C. 1996, *A&A*, 306, 677
- Lonsdale, C.J., Helou, G., Good, J., & Rice, W. 1985, *Catalogued Galaxies and Quasars in the IRAS Survey* (US GPO, Washington, D.C.)
- Ohtani, H., Uesugi, A., Tomita, Y., Yoshida, M., Kosugi, G., Noumaru, J., Araya, S., Ohta, K., & Mikayama, Y. 1992, *Memories of the Faculty of Science, Kyoto University, Series A of Physics, Astrophysics, Geophysics and Chemistry*, 38, 167
- Piçmiş, P. 1997, *RevMexAA (Serie de Conferencias)*, 6, 238
- Romanishin, W. 1990, *AJ*, 100, 373
- Ryder, S.D., & Dopita, M.A. 1994, *ApJ*, 430, 142
- Sandage, A., & Bedke, J. 1994, *The Carnegie Atlas of Galaxies* (Washington, DC: Carnegie Inst. of Washington with the Flintridge Foundation)

- Sandage, A., & Tammann, G. 1987, A Revised Shapley-Ames Catalog of Bright Galaxies
(Washington, DC: Carnegie Inst. Washington Pub. 635)
- Sauvage, M., & Thuan, T.X. 1992, ApJ, 396, L69
- Smith, B.J. 1994, AJ, 107, 1695
- Soifer, B.T., Sanders, D.B., Madore, B.F., Neugebauer, G., Danielson, G.E., Elias, J.H., Lonsdale,
C.J., & Rice, W.L. 1987, ApJ, 320, 238
- Stauffer, J.R. 1982, ApJS, 50, 517
- Tomita, A., Tomita, Y., & Saitō, M. 1996, PASJ, 48, 285
- Tully, R.B. 1988, Nearby Galaxies Catalog (Cambridge University Press, Cambridge)
- Walterbos, R.A.M., & Greenawalt, B. 1996, ApJ, 460, 696
- Wood, D.O.S., & Churchwell, E. 1989, ApJ, 340, 265
- Wunderlich, E., Klein, U., & Wielebinski, R. 1987, A&AS, 69, 487
- Xu, C. 1990, ApJ, 365, L47
- Young, J.S., Allen, L., Kenney, J.D.P., Lesser, A., & Rownd, B., 1996, AJ, 112, 1903

Fig. 1.— Comparison of $H\alpha$ EWs of this study with those of other studies for 7 galaxies. The diagonal line is shown for a reference.

Fig. 2.— R band (left) and continuum-subtracted $H\alpha+[N\ II]$ (right) images of the sample galaxies. North is at the top and east is at the left in each image. The images are trimmed to $3.3'\times 3.3'$, and the scale of $1'$ is shown in the $H\alpha$ image of NGC 681 and NGC 4045. The intensity is scaled logarithmically.

Fig. 3.— $\log[EW(H\alpha)]$ as a function of $\log(L_{FIR}/L_B)$ for early type spirals observed by us (closed circles) and Kennicutt (1983, 1992) (open circles). $H\alpha$ EWs of NGC 681 observed by us and Kennicutt (1983) are connected by a vertical line, and the mean of the two value is also shown with a cross. The dashed line is the least-square fit for galaxies with $EW(H\alpha) \geq 3\ \text{\AA}$.

Fig. 4.— $r_{e,H\alpha}/r_{e,R}$ as a function of $\log(L_{FIR}/L_B)$ for our sample galaxies plus one galaxy, NGC 7217, from the comparison sample which is classified as an early type spiral. The galaxies with vertical bar are barred galaxies (SB), and ones with horizontal bar are galaxies with companions.

Fig. 5.— $\log(L_{FIR}/L_{H\alpha})$ as a function of $\log(L_{FIR}/L_B)$ for galaxies with $\log(L_{FIR}/L_B) \geq -0.5$. The symbols are the same as in Fig. 3. The dashed line is the least-square fit.

Fig. 6.— $\log(L_{FIR}/L_{H\alpha})$ as a function of $r_{e,H\alpha}/r_{e,R}$. The sample is the same as in Figure 4.

Fig. 7.— The interaction parameter, IP, as a function of $\log(L_{FIR}/L_B)$ for (a) 87 early type spirals with $B_T^0 > 12$ mag and (b) our sample galaxies. The galaxies with cross are classified as peculiar in RC3.

Table 2. Global Propeties of the Comparison Galaxies

Galaxy	$\alpha(2000)$	$\delta(2000)$	Type	B_T^0	V_{GSR}	D_{25}	EW(H α)	Ref.
	(h m s)	($^{\circ}$ ' ")			(km s $^{-1}$)	(')	(\AA)	
(1)	(2)	(3)	(4)	(5)	(6)	(7)	(8)	(9)
NGC 681 ^a	014910.9	−102540	SAB(s)ab sp	12.50	1769	2.6	4±2	1
NGC 3055	095517.4	+041617	SAB(s)c	12.18	1698	2.1	59±4	2
NGC 6207	164304.4	+364959	SA(s)c	11.57	1010	3.0	35±4	1
NGC 6574	181150.7	+145850	SAB(rs)bc:	11.79	2441	1.4	27±5	1
NGC 7217	220752.2	+312135	(R)SA(r)ab	10.53	1162	3.9	6±2	1
NGC 7448	230003.7	+155857	SA(rs)bc	11.50	2370	2.7	40±4	1
NGC 7743	234421.6	+095604	(R)SB(s)0+	12.16	1807	3.0	3±3	1

^aNGC 681 is one of our sample galaxies and contained also in Table 1.

Note. — Col. (1): galaxy name; cols. (2)-(3): right ascension and declination (2000.0 coordinates) from RC3; col. (4): morphological type from RC3; col. (5): B_T^0 from RC3; col. (6): recession velocity V_{GSR} from RC3; col. (7): optical angular diameter calculated using D_{25} of RC3; col. (8): equivalent width of H α + [NII].

References. — (1) Kennicutt 1983; (2) Romanishin 1990.

Table 3. Observed EW(H α) and Other Results

Galaxy	EW(H α)	$\log f_{\text{H}\alpha}$	$\log L_{\text{H}\alpha}$	$r_{e,\text{H}\alpha}$	$r_{e,\text{H}\alpha}/r_{25}$	$r_{e,\text{H}\alpha}/r_{e,R}$
	(\AA)	($\text{erg s}^{-1} \text{ cm}^{-2}$)	(L_{\odot})	(kpc)		
(1)	(2)	(3)	(4)	(5)	(6)	(7)
the comparison galaxies						
NGC 3055	50 \pm 8.2	−11.7	7.51	1.4	0.21	0.65
NGC 6207	46 \pm 1.7	−11.6	7.21	1.4	0.24	0.96
NGC 6574	36 \pm 0.8	−11.8	7.96	1.9	0.24	0.75
NGC 7217	14 \pm 1.6	−11.5	7.31	3.0	0.31	1.21
NGC 7448	44 \pm 0.6	−11.6	7.97	3.5	0.28	1.21
NGC 7743	3 \pm 1.3	−12.7	6.56	0.4	0.03	0.10
the sample galaxies						
NGC 681 ^a	20 \pm 2.1	−12.1	7.16	2.5	0.28	1.05
NGC 1022	14 \pm 2.0	−11.9	7.12	0.4	0.06	0.17
NGC 2782	33 \pm 1.5	−11.7	7.84	1.0	0.06	0.30
NGC 2993	114 \pm 1.6	−11.6	7.91	0.7	0.12	0.56
NGC 3442	69 \pm 1.9	−12.1	7.10	0.7	0.33	1.00
NGC 3504	51 \pm 1.3	−11.2	7.66	0.6	0.07	0.29
NGC 3611	27 \pm 1.4	−12.0	7.09	0.6	0.09	0.50
NGC 3729	31 \pm 3.2	−11.6	7.15	1.5	0.26	0.79
NGC 4045	17 \pm 2.4	−12.1	7.13	2.2	0.21	0.90
NGC 4369	34 \pm 2.9	−11.7	7.02	0.5	0.11	0.44
NGC 4384	37 \pm 4.0	−12.2	7.33	1.2	0.18	0.58
NGC 5534	45 \pm 3.0	−11.8	7.73	1.8	0.26	0.95
NGC 5691	40 \pm 2.0	−11.7	7.60	1.2	0.18	0.62
NGC 5915	70 \pm 3.2	−11.6	7.93	1.5	0.18	0.77
NGC 7625	40 \pm 4.0	−11.8	7.47	0.9	0.17	0.57

^aNGC 681 is included for the comparison galaxies as well.

Note. — Col. (1): galaxy name; col. (2): observed equivalent width of H α + $[\text{NII}]$ and its error; col. (3): estimated H α + $[\text{NII}]$ line flux. See text for details; col. (4): estimated H α + $[\text{NII}]$ luminosity; col. (5): half-light radius of H α emission in kpc. See text for details; col. (6): the ratio of the half-light radius of H α emission to the optical radius, r_{25} , which is a half of D_{25} in Table 1 and Table 2; col. (7): the ratio of the half-light radius of H α emission to that of R band light.

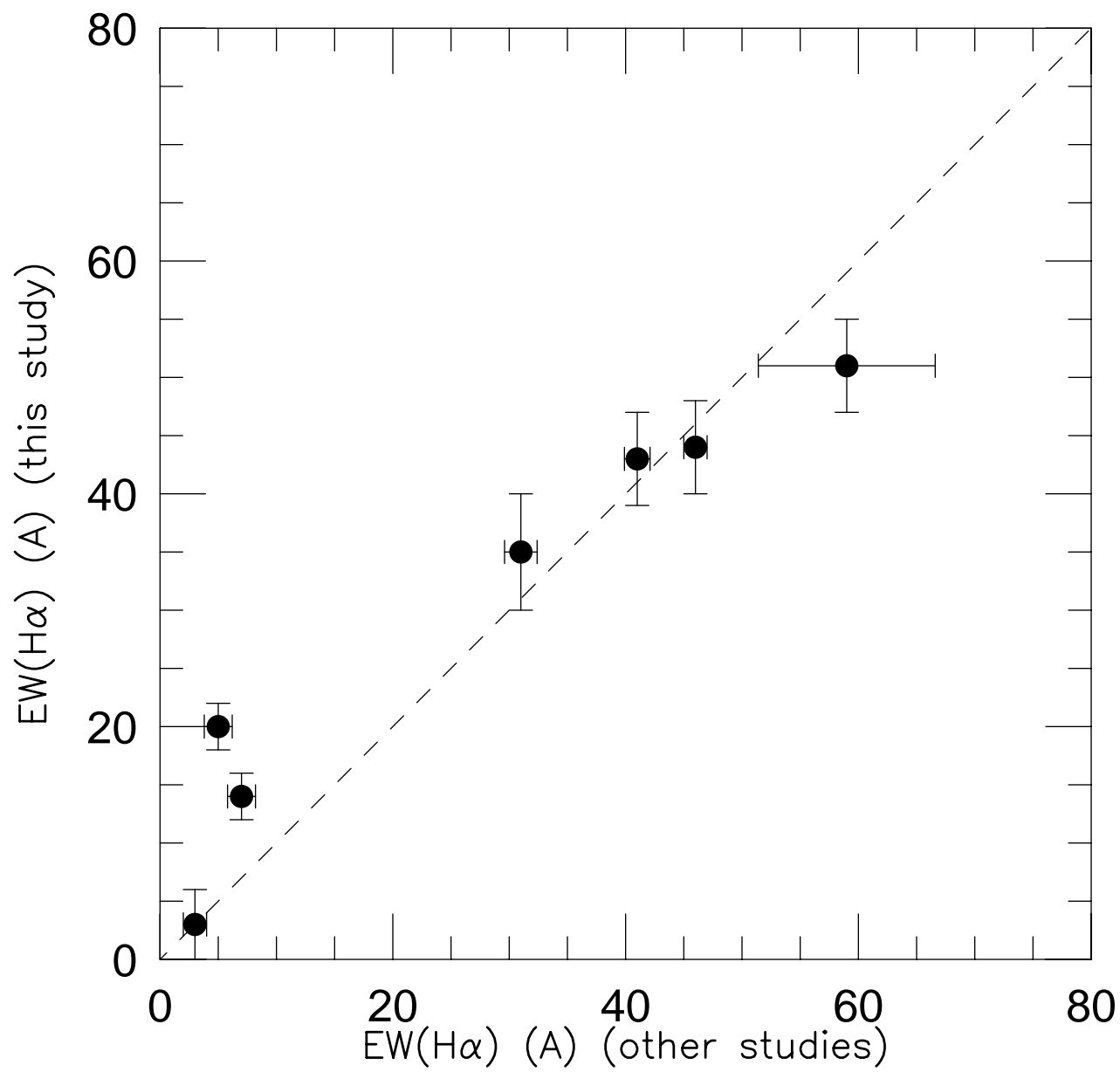


TABLE 1
GLOBAL PROPERTIES OF THE SAMPLE GALAXIES

Galaxy	$\alpha(2000)$ (h m s)	$\delta(2000)$ ($^{\circ}$ ' ")	Type	B_T^0	V_{GSR} (km s $^{-1}$)	D_{25} (')	D_{25} (kpc)	Inc. ($^{\circ}$)	$(B - V)_T^0$	$\log(L_{\text{FIR}}/L_B)$	$\log(L_B)$ (L_{\odot})	nuclear type	Ref.	other names
(1)	(2)	(3)	(4)	(5)	(6)	(7)	(8)	(9)	(10)	(11)	(12)	(13)	(14)	(15)
NGC 681	014910.9	−102540	SAB(s)ab sp	12.50	1769	2.60	17.9	55	0.74	−0.23	9.72			
NGC 1022	023832.8	−064041	(R')SB(s)a	11.94	1489	2.40	13.9	38	0.71	0.29	9.79			
NGC 2782	091405.5	+400652	SAB(rs)a pec	12.01	2551	3.50	34.7	46	0.61	0.03	10.23	HII	1,2	KUG 0910+403
NGC 2993	094548.4	−142208	Sa pec	12.65	2224	1.40	12.1	51	0.34	0.36	9.86	HII ^a	3	
NGC 3442	105308.2	+335436	Sa ?	13.64	1716	0.60	4.0	45	0.36	−0.07	9.23			Mrk 418, KUG 1050+341
NGC 3504	110310.8	+275825	(R)SAB(s)ab	11.51	1502	2.70	15.7	43	0.70	0.20	9.97	HII	2	KUG 1050+341
NGC 3611	111729.5	+043317	SA(s)a pec	12.31	1473	2.20	12.6	40	0.55	−0.15	9.63			
NGC 3729	113349.8	+530737	SB(r)a pec	11.91	1089	2.80	11.8	52	0.55	−0.45	9.53	HII	2	KUG 1131+534
NGC 4045	120242.0	+015844	SAB(r)a	12.52	1877	2.80	20.4	50	0.74	0.12	9.76			
NGC 4369	122435.9	+392257	(R)Sa(rs)a	12.27	1072	2.10	8.7	16	0.65	−0.05	9.37	HII	2	Mrk 439
NGC 4384	122512.0	+543017	Sa	13.38	2597	1.30	13.1	43	0.41	−0.04	9.70			Mrk 207
NGC 5534	141740.4	−072503	(R')SAB(s)ab pec:	12.68	2581	1.40	14.0	59	0.54	−0.06	9.97	HII	4	Mrk 1379
NGC 5691	143753.7	−002350	SAB(s)a: pec	12.52	1833	1.90	13.5	45	0.43	−0.19	9.74			
NGC 5915	152133.1	−130532	SB(s)ab pec	11.99	2265	1.90	16.7	48	0.26	0.05	10.14	HII	5	
NGC 7625	232030.8	+171341	SA(rs)a pec	12.67	1793	1.60	11.1	28	0.70	0.29	9.66	HII	6	

^aDurret & Bergeron (1988) classified this galaxy as a LINER based on the detection of [OI] λ 6300. But their line ratios, including [OI]/H α , are typical of HII regions.

NOTE.—Col. (1): galaxy name; cols. (2)-(3): right ascension and declination (2000.0 coordinates) from RC3; col. (4): morphological type from RC3; col. (5): B_T^0 from RC3; col. (6): recession velocity V_{GSR} from RC3; col. (7): optical angular diameter calculated using D_{25} of RC3; col. (8): optical diameter calculated using column (6) and (7), assuming $H_0 = 75$ km s $^{-1}$ Mpc $^{-1}$; col. (9): galaxy inclination in degrees. The inclination is calculated by the ratio of major to minor axes in RC3, R_{25} , using the equation shown in the Nearby Galaxies Catalog (Tully, 1988); col. (10): $(B - V)_T^0$ from RC3; col. (11): $\log(L_{\text{FIR}}/L_B)$ is calculated using B_T^0 in RC3 and f_{60} and f_{100} of *IRAS* data; col. (12): $\log(L_B)$ calculated using column (5) and (6); col. (13): nuclear spectral type; col. (14): references of col. (13); col. (15): other names.

REFERENCES.—1: Boer *et al.* 1992; 2: Ho *et al.* 1997; 3: Durret & Bergeron 1988; 4: Contini *et al.* 1998; 5: Pişmiş 1997; 6: Stauffer 1982.

